FEATURE ARTICLE

Shedding Light on Biomolecule Conformational Dynamics Using Fluorescence Measurements of Trapped Ions

Anthony T. Iavarone, Denis Duft, and Joel H. Parks*

The Rowland Institute at Harvard, 100 Edwin H. Land Boulevard, Cambridge, Massachusetts 02142

Received: August 1, 2006; In Final Form: September 13, 2006

Biomolecule conformational change has been widely investigated in solution using several methods; however, much less experimental data about structural changes are available for completely isolated, gas-phase biomolecules. Studies of conformational change in unsolvated biomolecules are required to complement the interpretation of mass spectrometry measurements and in addition, can provide a means to directly test theoretical simulations of biomolecule structure and dynamics independent of a simulated solvent. In this Feature Article, we review our recent introduction of a fluorescence-based method for probing local conformational dynamics in unsolvated biomolecules through interactions of an attached dye with tryptophan (Trp) residues and fields originating on charge sites. Dye-derivatized biomolecule ions are formed by electrospray ionization and are trapped in a variable-temperature quadrupole ion trap in which they are irradiated with either continuous or short pulse lasers to excite fluorescence. Fluorescence is measured as a function of temperature for different charge states. Optical measurements of the dye fluorescence include average intensity changes, changes in the emission spectrum, and time-resolved measurements of the fluorescence decay. These measurements have been applied to the miniprotein, Trp-cage, polyproline peptides and to a β-hairpin-forming peptide, and the results are presented as examples of the broad applicability and utility of these methods. Model fits to Trp-cage fluorescence data measured as a function of temperature provide quantitative information on the thermodynamics of conformational changes, which are reproduced well by molecular dynamics. Time-resolved measurements of the fluorescence decays of Trp-cage and small polyproline peptides definitively demonstrate the occurrence of fluorescence quenching by the amino acid Trp in unsolvated biomolecules.

1. Introduction

Living organisms rely on proteins and other biopolymers to carry out a wide range of biochemical processes, such as recognition, transport, synthesis, and degradation, with high specificity and efficiency. Although polymers can potentially take on several possible conformations due to rotations about single bonds, proteins have the capability to cooperatively fold into a unique, native structure that exhibits a specific biological activity.[1,2] Understanding the details of how a stable three-dimensional structure is produced from a given sequence of amino acids remains a major challenge in physical chemistry and molecular biology and has special relevance to the design of industrial enzymes and protein therapeutics[3] and to the prevention, diagnosis, and treatment of several diseases, which are believed to involve protein misfolding and aggregation.[4−7] In condensed phase, structures can be determined at atomic-level resolution using X-ray crystallography and NMR, and the kinetics of folding and unfolding events can be studied using time-resolved spectroscopy. The measurements of completely isolated biomolecules in gas phase that complement condensed-phase measurements are useful for elucidating the role of the solvent environment in producing the native structure and dynamics. Such measurements can be directly compared with theoretical calculations as a means to test molecular dynamics (MD)[8,9] force fields independent of any explicitly or implicitly simulated solvent. These simulations are simplified in gas phase in which the dynamics depend only on interactions between the different parts of the biopolymer and not on interactions between the molecule and surrounding solvent. Gas-phase experiments can also provide insight into the mechanisms through which product ions are formed during tandem mass spectrometry (MS/MS) measurements of protein and peptide ions. MS/MS is an invaluable tool for proteomics, because it can rapidly identify proteins in complex mixtures by providing partial or total sequence information through the fragmentation of gas-phase ions.[10,11] It can also provide information that is not directly available from the DNA sequence, such as the identity and location of posttranslational modifications.[12,13] The amount of information that can be obtained from MS/MS of a large biomolecule (i.e., the abundance and locations of bond cleavages) is believed to depend in part on the higher order structure and/or dynamics of the gas-phase ions.[14−17]

Large biomolecules can be formed as ions in the gas phase using electrospray ionization (ESI)[18] or matrix-assisted laser desorption/ionization (MALDI).[19,20] In particular, ESI has the capability to form extensively charged ions that makes possible the measurement of high molecular weight species without

* Corresponding author. E-mail: parks@rowland.harvard.edu. Phone: (617) 497-4653. Fax: (617) 497−4627.

10.1021/jp064933e CCC: $33.50
Published on Web 11/09/2006

Anthony T. Iavarone earned a B. S. in Chemistry from the University of California, Irvine in 1996. After working in industry as an analytical chemist, he pursued graduate studies in Chemistry at the University of California, Berkeley under the guidance of Professor Evan Williams and earned a Ph.D. in 2004. His graduate research focused on analyte charging and sensitivity in electrospray ionization and charge state and metal cation effects on the dissociation of multiply charged proteins and peptides. He is currently a Postdoctoral Fellow at the Rowland Institute at Harvard and is interested in the introduction of new methods for understanding life at the molecular level.

Denis Duft earned an M. S. in Physics from Freie Universität Berlin in 2000 under the guidance of Professor Ludger Wöste and a Ph.D. of Sciences in Physics from Technische Universität Ilmenau in 2006 under the guidance of Professor Thomas Leisner. His graduate research focused on the microphysics of clouds as studied on single, electrodynamically levitated microdroplets, including experimental studies of their freezing behavior, refractive index, and stability with respect to Coulombic fission. He is currently a Postdoctoral Fellow at the Rowland Institute at Harvard and is interested in understanding the nature of electron transfer in chemical reactions and revealing the molecular secrets of human life.

Joel H. Parks earned B. S. and Ph.D. degrees in Physics in 1959 and 1969, respectively, from the Massachusetts Institute of Technology. After undergraduate studies, he performed research at Polaroid Corporation under the guidance of Dr. Edwin H. Land on various camera related technologies and teaching machine concepts. His graduate research under the guidance of Professor Ali Javan included measurement of collisional energy transfer in rare gases, measurement of the interaction of laser fields with Zeeman-tuned atomic levels, high-resolution spectroscopy of ultraviolet-stimulated emission in molecular nitrogen, and theoretical studies of superfluorescent emission bandwidth and nonlinear behavior of atom-field interactions within lasing media. At the University of Southern California in 1969, he studied energy transfer in polyatomic molecules, laser-induced electronic processes that damage dielectric surfaces, surface wave techniques for measuring ultra-weak infrared surface absorption coefficients in alkali halides, and the theory of high-gain laser amplifiers for broad band optical fields. As a member of the Senior Staff at Avco Everett Research Laboratory in 1976, he discovered new species for visible lasers and demonstrated mercury monohalide lasers HgCl and HgBr. He was one of the original research staff of the Rowland Institute at its founding in 1981 and set up a lab to investigate excited states of atoms and molecules on surfaces. He measured the evolution of collective mode resonances in small sodium clusters as a function of atom number and the growth and charge distribution within atomic cluster ions stored in rf quadrupole traps. He is currently a Senior Fellow at the Rowland Institute at Harvard and is studying conformational changes in trapped biomolecule ions using fluorescence and the measurement of structural transitions in trapped atomic cluster ions using electron diffraction.

exceeding the upper mass-to-charge (m/z) limits of mass spectrometers such as ion traps. Several methods have been developed to probe the structures of biomolecule ions in gas phase including ion mobility spectroscopy,[21−26] ion−molecule reactions, such as proton transfer[27] and hydrogen/deuterium exchange,[26,28] dissociation induced by blackbody radiation[29] or captured electrons,[30,31] and infrared photodissociation spectroscopy.[32,33] These methods have a demonstrated ability to detect large-scale changes in the overall conformation of biopolymer ions.

In our lab, we have been developing fluorescence-based methods[34] to probe *local* conformational changes or fluctuations in trapped gas-phase biomolecule ions. Initially, these methods were applied to studies[35] of oligonucleotide duplex melting by measuring fluorescence resonance energy transfer (FRET) between donor and acceptor dyes attached to the chain termini. The observation[36,37] of electron autodetachment from the multiply charged oligonucleotide anions was identified in these studies for the first time. The autodetachment process was found to be an interesting mechanism that was quite sensitive to temperature, charge state, and base sequence. However, depending on the base sequence, the electron loss process was associated with bond cleavage and quenching, which complicated the fluorescence analysis. Lower loss rates could be achieved by reducing the temperature and charge state, but this seriously constrained the range in which the gas-phase oligonucleotides could be studied. Fluorescence methods have since been applied to charged proteins,[38,39] and it was found that simpler configurations with a single fluorophore attached to the biomolecule were sufficient to observe conformational changes. This methodology relies on changes in the fluorescence emission intensity or decay time that are induced by a strong interaction between the covalently attached dye and an amino acid, tryptophan (Trp), which quenches the dye fluorescence. Quenching of the fluorescence through photoinduced electron transfer (PET) results in nonradiative decay of the excited dye. This approach, which has been used in solution for both ensemble and single molecule studies,[40−52] is sensitive to angstrom-scale conformational fluctuations owing to the exponential dependence of the PET rate on the fluorophore-quencher separation.[53,54] In this Feature Article, we describe the application of this method to the characterization of conformational changes and fluctuations in unsolvated ions of proteins and peptides. In contrast to solution measurements, the kinetic time scale is not diffusion limited, and the attached dye probes the biomolecular ion through interactions not only with Trp residues but also with the Coulomb fields of the charges. These measurements are not used to directly determine high-resolution structures of the gas-phase biomolecules or the unfolding pathways. Instead, the fluorescence data measured as a function of temperature are used to thermodynamically and/or kinetically characterize structural changes. Experiments are performed on different charge states and on selected single-point mutants to isolate the effects of individual electrostatic interactions on the biomolecule stability and dynamics. The first *time-resolved* measurements of unsolvated biomolecular ions derivatized with a fluorescent dye are presented that clearly demonstrate the occurrence of fluorescence quenching through interactions with Trp.

2. Experimental Methods

2.1. Nanoelectrospray Ionization Mass Spectrometry. Details of the instrumentation have been published elsewhere.[34,39] In brief, experiments are performed on a custom-built quadrupole ion trap. Droplets and ions formed by nanoelectrospray (nanoES) are sampled from atmospheric pressure through a stainless steel capillary maintained at 333 K and guided through an octupole ion guide into a quadrupole ion trap that can be heated to temperatures as high as ∼443 K. The ions of interest are isolated by ejecting ions occurring at higher or lower m/z ratios using radio frequency (RF) ramping and stored wave form inverse Fourier transform (SWIFT).[55,56] The background helium gas pressure is maintained at $\sim 3 \times 10^{-6}$ Torr and is pulsed to $\sim 2 \times 10^{-4}$ Torr for ion loading and thermalization. (The pressure within the trap is ∼30−35-fold higher because of the conductance limits of the trap apertures.) Ions are thermalized in the trap for 1 s before measuring fluorescence at $q_z = 0.50$. The trapped ions undergo $>10^5$ collisions that equilibrate them with the bath gas, which is maintained at the temperature of the trap. After measuring fluorescence, the ions are ejected and detected using an electron multiplier.

2.2. Fluorescence Spectroscopy. The apparatus developed for these fluorescence measurements, which shows the primary optical components in the laser beam path, is shown in

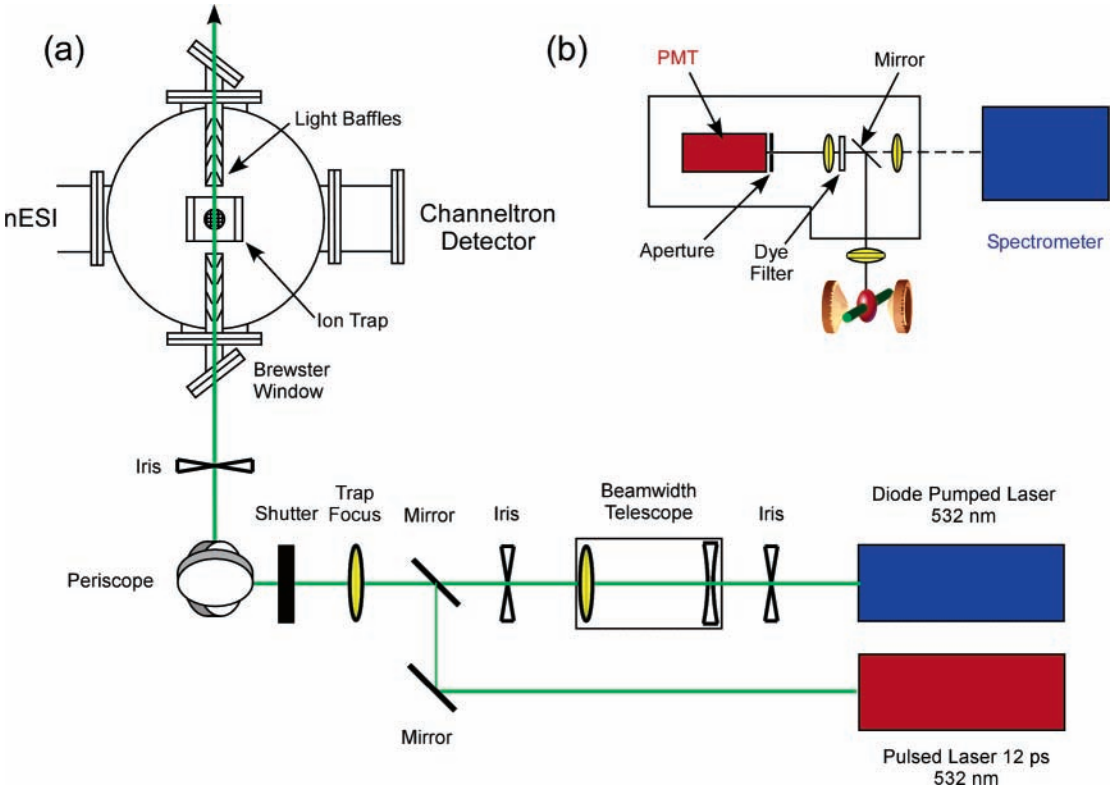

Figure 1. Diagrams of optics for (a) excitation and (b) detection of fluorescence from trapped gas-phase ions.

Figure 1. The excitation optics shown in Figure 1a include a beam-forming telescope to optimize overlap of the laser beamwidth with the trapped ion cloud. The various irises and light baffles are required to minimize the radiation forward-scattered by optical elements that would be subsequently scattered by the trap electrodes into the detection optics. Fluorescence intensity measurements are performed by irradiating the trapped ions with 532 nm light (frequency doubled) from a continuous wave Nd:YAG laser (Millennia VIs, Spectra-Physics, Irvine, CA) for 100 ms at an intensity of 130 W/cm^2. The Gaussian laser beam diameter has been reduced to $\sim$220 μm to minimize light scattering on the trap apertures. The laser-ion cloud overlap is further optimized by alignment of the laser and adjustment of the DC bias voltage applied to the trap endcaps that alters the cloud position. As shown in Figure 1b, fluorescence is collected through a 25 mm diameter triplet lens and passes through a band-pass filter ($\sim$550$-$595 nm passed) (Chroma, Rockingham, VT) before impinging on a Ga$-$As photomultiplier (Hamamatsu, Hamamatsu City, Japan). A sharp cutoff long wave filter (Chroma, Rockingham, VT) is required to minimize detection of scattered laser radiation.

Twenty-five replicate measurements are performed for each data point, and each set of measurements is performed at least two times on different days. The day-to-day reproducibility of absolute intensity is within $\pm$ 20%. The fluorescence data routinely exhibit a signal-to-noise (S/N) ratio in the range of 100$-$400 for $\sim$200 ions in the laser interaction volume ($\sim 2 \times 10^{-5}$ cm^3). The high S/N achieved by the optics design in Figure 1 enables us to perform filtered fluorescence measurements on small ion numbers. An example of this sensitivity is indicated in Figure 2 for measurements of Rhodamine 640 fluorescence vs the number of ions excited by 100 mW light of 532 nm in a 220 μm beamwidth. The use of such small numbers of ions minimizes space charge interactions resulting in higher resolution mass spectrometry measurements of the trapped ions, increased density ion clouds, and more reliable ion trajectory simulations.

The dye fluorescence spectrum can be measured by adjusting the mirror shown in Figure 1b to focus the fluorescence on the entrance slit of a 0.3 m/f4 spectrometer (Andor, Belfast, Ireland). The spectrum is detected by a linear 1600 element electron multiplying charge-coupled device (CCD) (Andor, Belfast, Ireland). Excitation at 532 nm is similar to filtered intensity measurements, and the spectrum is measured between 540 and 700 nm. The spectra are recorded using Andor-Solis software, and the fluorescence bandwidth and center wavelength shift are measured as a function of temperature for each charge state. These parameters are intrinsic to the biomolecule and help to interpret the dynamics.

Several fluorescent dyes were screened at the outset of this research to identify those whose radiative properties are not significantly altered upon desolvation and heating. The dipyrromethene boron difluoride (BODIPY) analogue of tetramethylrhodamine (BoTMR) was found to be ideal because it is uncharged in solution, excited efficiently at 532 nm, and emits with high quantum yield (>80%) exhibiting minimal solvent and temperature dependence throughout the visible spectrum.[35] The high-fluorescence S/N obtained with this dye allows for excitation using low-laser intensities to minimize heating of the gas-phase biomolecules. The laser-induced temperature increase of trapped polypeptide ions in the helium background gas has been measured to be $\leq$ 3 K for an intensity of 130 W/cm^2. Clearly, the laser-induced heating of the ions would be more severe if a natural fluorophore such as Trp, which has small quantum yield ($\sim$20%), were used instead of BoTMR.

2.3. Time-Resolved Fluorescence. The pulsed laser shown in Figure 1a provides excitation using 532 nm light (frequency doubled) from a mode-locked, diode-pumped, solid-state Nd:YAG laser (Vanguard 2000-HM532, Spectra-Physics). The

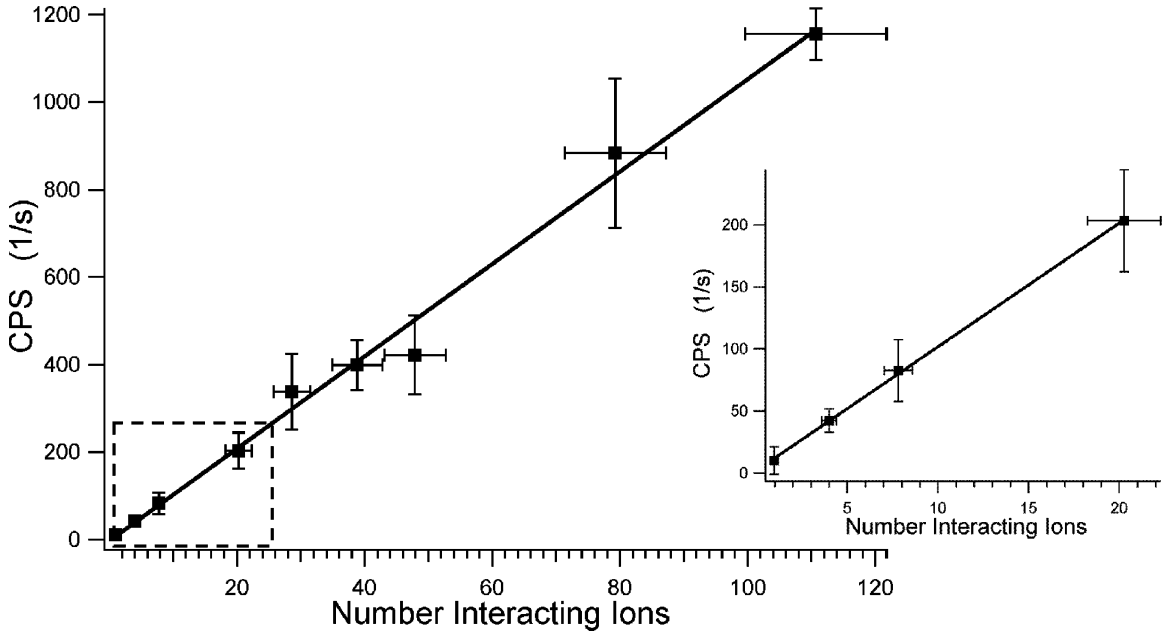

Figure 2. Background-subtracted fluorescence intensity measured as a function of the number of ions of the fluorescent dye, Rhodamine 640, in the laser interaction volume. The laser beam diameter is 220 μm (fwhm). The inset shows details for $\leq$20 ions.

repetition rate is reduced from 80 to 20 MHz through pulse picking by a transverse field modulator (Conoptics, Danbury, CT) and the pulse width is 12 ps (full width at half-maximum, fwhm). Emitted fluorescence is detected as described in the preceding section. A histogram-accumulating real-time processor (TimeHarp 200, PicoQuant, Berlin, Germany) is used for time-correlated single photon counting. The average detected count rate is maintained below 1% of the excitation rate to maintain single photon counting statistics (i.e., to ensure a low probability of detecting more than one photon per cycle). The resulting fluorescence decay curves are deconvoluted and fit by a stretched exponential model implemented in the FluoFit data analysis package (version 4.0, PicoQuant).

2.4. Materials. Derivatized peptides are commercially synthesized (BioMer Technology, Concord, CA) and purified by reversed-phase HPLC to a stated purity of >70% prior to shipment. The BODIPY analogue of tetramethylrhodamine (BoTMR) is obtained from Invitrogen (Carlsbad, CA) with or without an aminohexanoate linker (cat. no. D6117 and B10002, respectively; the former is used unless otherwise noted). The BoTMR chemical structures and excitation and emission spectra have been published elsewhere.[35,57] Attachment of BoTMR to peptides does not significantly alter the emission or excitation spectra (data not shown). Electrospray solutions contain the analyte at 10^{-5} M in water or 50% acetonitrile/50% water.

3. Computational Methods

The MD simulations used for dye−Trp-cage analysis are described in detail elsewhere.[58,59] Briefly, simulations are performed using GROMACS[59] with the OPLS/AA force field. The NMR structure[60] is used as the initial conformation, and energy minimization is performed by steepest descents. Replica exchange[61] is a method to overcome the problem of quasi-ergodicity in molecular dynamics simulations arising from trapping in local minima for long times and has proven to be a useful method for sampling phase space. Replica exchange simulations of 500 ns were performed at 16 different temperatures between 280 and 445 K. Calculations of the $(M + 2H)^{2+}$ ion were performed for two sets of protonation sites at Gln5 and Arg16 (Q5R16) and also at Lys8 and Arg16 (K8R16). For the $(M + 3H)^{3+}$ ion, calculations included a third charge on the N-terminus in each set (N1 Q5R16 and N1 K8R16). The carboxylic acid of the side chain of Asp9 is modeled in its neutral (protonated) form. No cutoff is used for Coulomb and van der Waals interactions, because all interactions are explicitly calculated in vacuo ($\epsilon = 1$). The total number of hydrogen bonds formed between all of the backbone carbonyl oxygens and any other part of the molecule is calculated by summing the fractions of instances each carbonyl oxygen is found to be participating in a hydrogen bond during the simulation. The total number of instances is 500 000, one for each ps of simulation time. The "global" minimum energy structures are determined as described previously.[58] Root-mean-square deviations (RMSD) used to compare different unsolvated structures with NMR structures are calculated using the α-carbons of the polypeptide backbone.

4. Fluorescence Results and Discussion

4.1. Trp-Cage: Miniprotein Stability in Gas Phase and in Solution. Andersen and co-workers[60] reported a 20-residue construct resulting from truncation and mutation of exendin-4, which is a peptide isolated from Gila monster saliva that exhibits stable secondary and tertiary structure in aqueous solution. This protein, Trp-cage, is advantageous for the initial demonstration of the fluorescence probe, because its structure has been determined at high resolution by NMR,[60] it is sufficiently small for chemical synthesis to expedite the production of sequence variants and site-specific derivatization with fluorescent dyes, and its main chain conformation and side chain packing are reproduced by MD as demonstrated by several groups.[58,62−68] The sequence used in our studies, H_2N-NLYIQWLKDGGPSS-GRPPPSK(BoTMR)-ONH_2, is the same as that reported by Andersen and co-workers (sequence "TC5b")[60] except that the C-terminus is amidated, and a lysine has been added to the C-terminal end to allow for conjugation of the dye via the side chain ϵ-amine. The unfolding temperature, T_m, measured[69] for this molecule in aqueous solution in our lab is 323 K, which is slightly higher than that of unmodified Trp-cage (314 K).[60,70] The $(M + 2H)^{2+}$ and $(M + 3H)^{3+}$ charge states are formed by nanoES (Figure 3a). As shown in the example, isolation spectrum and fluorescence data of the $(M + 3H)^{3+}$ ion in Figure

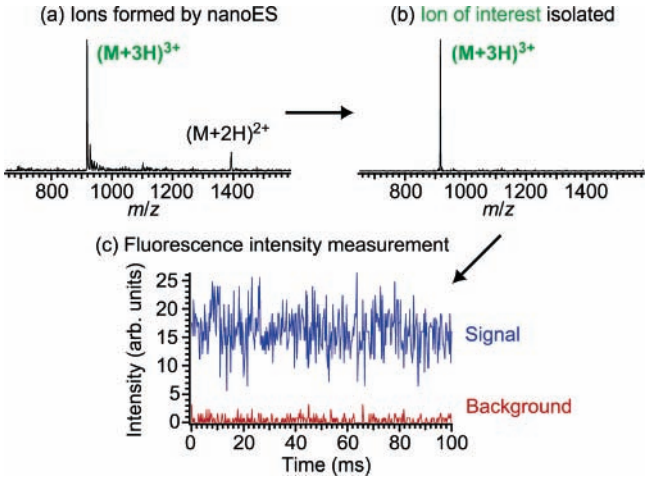

Figure 3. Sample experimental sequence for fluorescence intensity measurement of dye-derivatized Trp-cage ions. (a) Charge state distribution formed by nanoES. (b) Isolation mass spectrum of the $(M + 3H)^{3+}$ ion. (c) Fluorescence intensity of the $(M + 3H)^{3+}$ ion measured over 100 ms (blue) compared with background noise due to scattered excitation light (red).

3, panels b and c, respectively, the mass spectral resolution is sufficient to isolate and identify the unsolvated, nonadducted protein ions, and the detected fluorescence intensity excited by the continuous wave 532 nm laser is well above the background noise (scattered light from the excitation laser).

The fluorescence intensity per trapped $(M + 2H)^{2+}$ ion is essentially constant between 303 and 403 K and then decreases by 30% upon further heating to 438 K (Figure 4a). For the $(M + 3H)^{3+}$, the fluorescence intensity is unchanged from 303 to 363 K but then decreases by 75% upon further heating to 438 K (Figure 4b). Thus, the temperature-dependent fluorescence of these protein ions exhibits a strong dependence on charge state. In contrast, singly charged ions of the BoTMR dye, which is not attached to the protein, exhibit a constant fluorescence intensity over the entire temperature range (Figure 4c) indicating that the changes observed in Figure 4, panels a and b, are caused by interactions between the dye and the protein and not caused by the intrinsic temperature-dependent photophysics of the dye.

A model[71] describing the temperature dependence of fluorescence quenching in the gas phase was derived assuming two-state unfolding behavior. Briefly, it is assumed that the quencher, Trp, becomes more accessible to interaction with BoTMR as the fraction of unfolded proteins increases with increasing temperature. Quenching is taken to be absent in the folded state and to occur with a rate constant, k_q, in the unfolded state:

$$\phi/\phi_0 = \chi_f + \frac{1}{1 + k_q\tau_0}\chi_u \qquad (1)$$

The fluorescence intensity, I, is proportional to ϕ, the quantum yield at a given temperature, and ϕ_0 is the quantum yield for the fully folded ensemble. χ_f and χ_u are the protein fractions in the folded and unfolded states, respectively, where $\chi_f = [1 + \exp(-\Delta G/kT)]^{-1}$ and $\chi_u = 1 - \chi_f$. Fits of this model to the data are performed by varying the change in enthalpy, ΔH, and entropy, ΔS, defining the free energy change, $\Delta G = \Delta H - T\Delta S$. These fits that are shown in Figure 4 yield the thermochemical parameters, ΔH and ΔS, associated with the conformational change. The resulting fits display an insensitivity to different models used to estimate k_q, because in each case, it is found that $k_q\tau_0 \gg 1$, a consequence of the gas-phase kinetics.

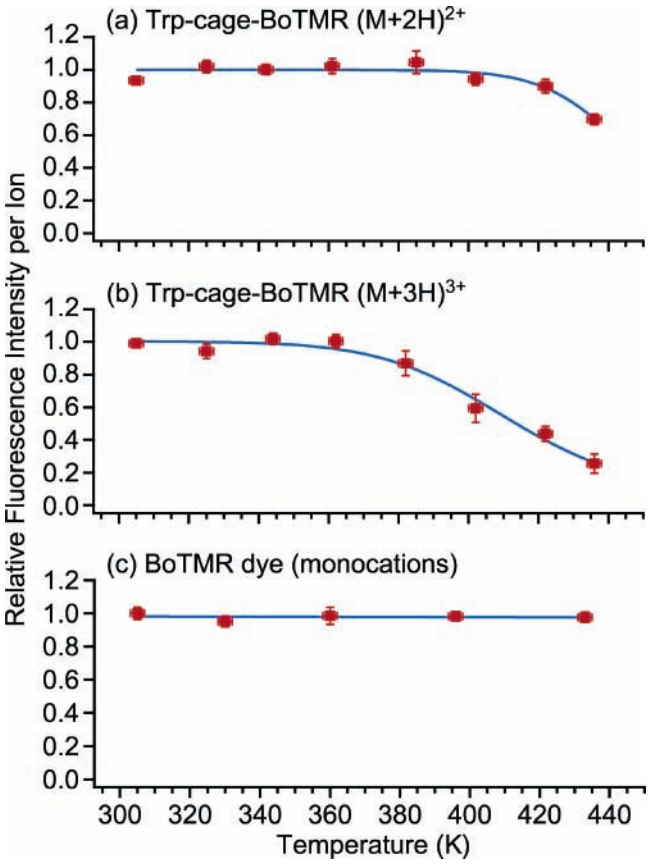

Figure 4. Normalized fluorescence intensity per ion vs temperature for the (a) $(M + 2H)^{2+}$ and (b) $(M + 3H)^{3+}$ ions of Trp-cage-BoTMR and (c) monocations of BoTMR dye. Measured data points are denoted by red markers and model fits to the data are delineated by blue curves. Intensities are normalized to 303 K values.

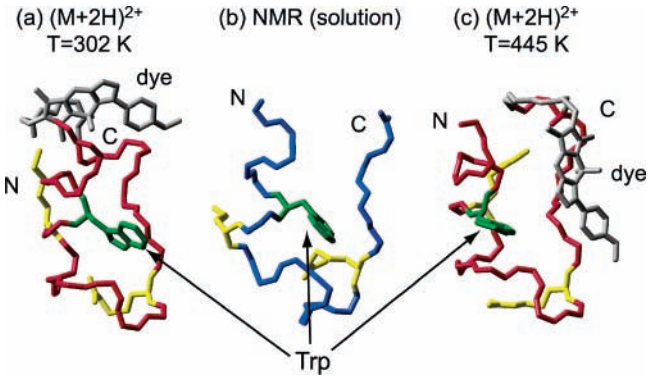

Figure 5. Selected structures resulting from simulations of the $(M + 2H)^{2+}$ ion (K8R16 charge configuration) of Trp-cage-BoTMR (red backbone) at (a) 302 K and (c) 445 K compared with (b) the solution structure determined by NMR (blue backbone; ref 60). The C- and N-termini are denoted by "C" and "N", respectively, and the BoTMR dye, Trp, and charged residues are gray, green, and yellow, respectively.

4.1.1. Molecular Dynamics/Fluorescence Comparison: Structure. Representative structures resulting from MD simulations of the $(M + 2H)^{2+}$ and $(M + 3H)^{3+}$ ions (K8R16 and N1K8R16 charge configurations, respectively) of Trp-cage derivatized with BoTMR are shown in Figures 5 and 6, respectively, alongside the NMR structure.[60] The backbone RMSD of the $(M + 2H)^{2+}$ and $(M + 3H)^{3+}$ ions at 302 K from the NMR structure are 4.53 and 3.76 Å, respectively. It is apparent that the overall backbone structures of the unsolvated ions at this temperature are roughly similar to that of the native protein. At 445 K, the

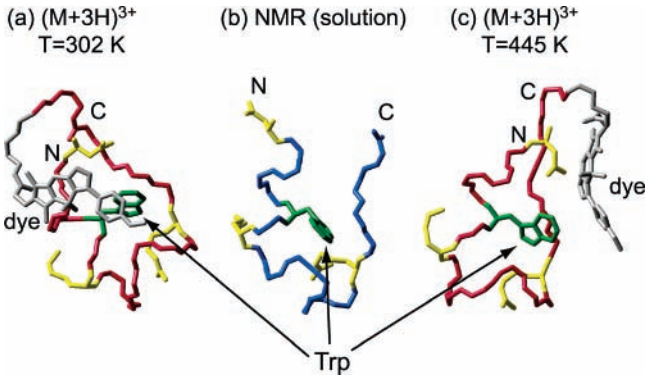

Figure 6. Selected structures resulting from simulations of the $(M + 3H)^{3+}$ ion (N1K8R16 charge configuration) of Trp-cage-BoTMR at (a) 302 K and (c) 445 K compared with (b) the solution structure determined by NMR (ref 60). The C- and N-termini are denoted by "C" and "N", respectively. The color scheme is the same as that in Figure 5.

backbones of the 2+ and 3+ ions remain largely unchanged (Figures 5c and 6c) with RMSD = 4.74 and 3.79 Å, respectively.

These calculations indicate that the removal of the solvent and the addition of two or three protons do not significantly alter the overall main chain conformation at this temperature and on this time scale, although side chain rotation is evident. The calculated structures remain relatively compact at the higher temperature as shown in Figures 5c and 6c. This is consistent with the unfolded conformations for Trp-cage in solution calculated by Pande and co-workers[63] and suggests that the fluorescence is probing the temperature dependence of the conformational fluctuations of secondary structure rather than large scale changes of the tertiary structure. The backbone of the $(M + 2H)^{2+}$ ion undergoes slight fluctuations upon heating to 445 K (Figure 5c); however, that of the $(M + 3H)^{3+}$ can undergo distortions in which the cage structure surrounding the Trp is opened up, as shown in Figure 6c. Thus, the temperature-dependent conformational dynamics exhibit a charge state dependence that is qualitatively consistent with that observed in the experiments.

4.1.2. Molecular Dynamics/Fluorescence Comparison: Energetics. The ΔH and ΔS, derived from model fits to the data for the $(M + 2H)^{2+}$ and $(M + 3H)^{3+}$ ions of Trp-cage-BoTMR, are shown in Table 1. The enthalpy changes derived from model fits to the data for the $(M + 2H)^{2+}$ and $(M + 3H)^{3+}$ ions of Trp-cage-BoTMR are 182% and 52%, respectively, larger than those in solution. The effects of Coulombic repulsion on conformational change of unsolvated, multiply charged proteins are estimated by considering the Coulombic energy released due to an increase in separation between like charges. The difference, ΔE_{Coul}, between the Coulombic energies of the final (unfolded) and initial (folded) states is given by

$$\Delta E_{Coul} = E_{unf} - E_{fold} < 0 \qquad (2)$$

E_{fold} and E_{unf} are approximated by summing the pairwise interactions between point charges in the folded and unfolded states, respectively (using a dielectric polarizability of 1.3).[72] The distances between the charge sites in the folded and unfolded states are derived from MD simulations (described above) performed at 302 and 445 K, respectively. The measured enthalpy change, ΔH, is just the sum of the intrinsic enthalpy of unfolding, ΔH_{int}, and ΔE_{Coul}. Thus, the values of ΔH_{int} shown in Table 1 are calculated as $\Delta H_{int} = \Delta H - \Delta E_{Coul}$. For the purpose of calculating ΔH_{int}, K8 and R16 were used as charge locations for the $(M + 2H)^{2+}$ ion and N1, K8, and R16 were used for the $(M + 3H)^{3+}$ ion. The values of ΔH_{int} for the $(M + 2H)^{2+}$ and $(M + 3H)^{3+}$ charge states are ~1% and ~14% higher, respectively, than the corresponding values of ΔH (Table 1).

Hydrogen bonds are likely to play an important role in stabilizing the protein structure in gas phase owing to the several hydrogen bond donor and acceptor groups, such as amide nitrogens and carbonyl oxygens, of the polypeptide backbone. Upon the removal of solvent water, which can form competing *inter*molecular hydrogen bonds with solvent-exposed groups on the protein, new *intra*molecular hydrogen bonds may be formed among different parts of the protein, which may provide additional stability to the folded structure.[58,73] Such hydrogen bond formation has been shown to stabilize unsolvated noncovalent complexes.[74]

The numbers of hydrogen bonds in the $(M + 2H)^{2+}$ and $(M + 3H)^{3+}$ ions derived from MD simulations are plotted as a function of temperature in Figure 7. For the K8R16 charge configuration of the $(M + 2H)^{2+}$ ion, the number of hydrogen bonds decreases by 2.4 between 302 and 445 K, which corresponds to ~50−100 kJ/mol based on published hydrogen bond energies.[75,76] A direct quantitative comparison between the decrease in the calculated number of hydrogen bonds and the enthalpy change derived from model fits to the data for the $(M + 2H)^{2+}$ ion (Table 1) is difficult because the conformational change is incomplete over this temperature range, as indicated by the small changes in fluorescence measured at the highest temperatures for this ion (Figure 4a). For the $(M + 3H)^{3+}$ configuration, N1K8R16, the calculated number of hydrogen bonds decreases by 1.9 between 302 and 445 K, corresponding to ~40−80 kJ/mol.[75,76] This result agrees reasonably well with the value of ΔH_{int} for the $(M + 3H)^{3+}$ N1K8R16 configuration, 84 (± 11) kJ/mol (Table 1). The smaller uncertainties in the derived thermochemical parameters of the $(M + 3H)^{3+}$ as compared with those of the $(M + 2H)^{2+}$ ion (Table 1) are due to the better model fits to the data that result from the more complete conformational change of the higher charge state over the temperature range investigated (Figure 4b).

The ΔS for the $(M + 2H)^{2+}$ and $(M + 3H)^{3+}$ ions are 98% and 16% larger, respectively, than that measured in solution (Table 1). One possible contributor to the discrepancies between solution and gas phase is the lack of a "water ordering effect".[1] In solution, an unfolding event that results in a greater exposure of hydrophobic residues to solvent imposes an entropic cost due to the increased ordering of water molecules around the newly exposed nonpolar surface. Because the water molecules cannot form hydrogen bonds with the hydrophobic surface, they form an ordered network around it by hydrogen bonding with each other. The discrepancies between solution and gas-phase entropy changes also may be due in part to changes in the conformational flexibility of the folded and/or unfolded states that stem from the loss of shielding by solvent. In the absence of water, the positive charges (e.g., the protonated arginine side chain) are expected to be solvated by polar functional groups such as backbone carbonyl oxygens. The coordination of polar backbone groups around the charges would effectively increase the local order of the polypeptide backbone and charged side chain(s).

Several types of interactions may potentially confer stability to unsolvated proteins including hydrogen bonds, salt bridges, and van der Waals interactions.[1,2] In particular, a salt bridge can potentially contribute ~60 kJ/mol in unsolvated peptides depending on the basicities of the participating groups.[77−79]

TABLE 1: Thermochemical Parameters Derived from Fluorescence Measurements[a]

analyte	charge state	electrospray solvent	ΔH (kJ/mol)	ΔH_{int} (kJ/mol)[b]	ΔS (J/mol·K)
Trp-cage-BoTMR	$(M + 2H)^{2+}$	aqueous	137 ± 52	139 ± 52	307 ± 120
Trp-cage-BoTMR	$(M + 3H)^{3+}$	aqueous	74 ± 11	84 ± 11	180 ± 27
solution[c]			48.6		155

[a] Stated errors are ± one standard deviation from the mean. [b] Calculated using charge locations K8 and R16 for the $(M + 2H)^{2+}$ ion and N1, K8, and R16 for the $(M + 3H)^{3+}$ ion. [c] Literature values (ref 70).

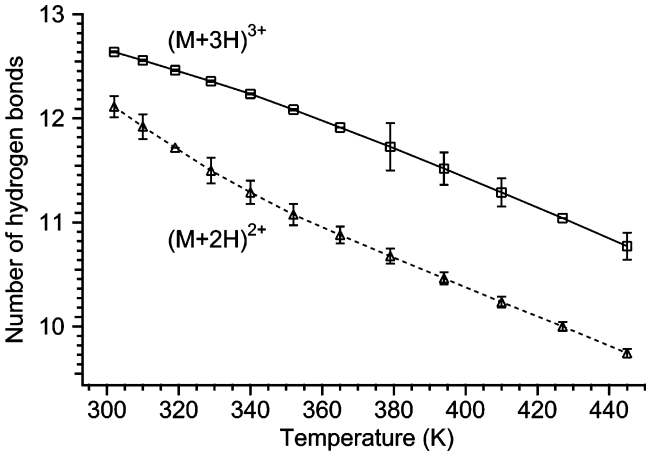

Figure 7. The total number of hydrogen bonds between the backbone carbonyl oxygens and any other part of the molecule for the $(M + 2H)^{2+}$ (K8R16 configuration; triangles) and $(M + 3H)^{3+}$ (N1K8R16; squares) ions of Trp-cage-BoTMR, as determined from molecular dynamics simulations. The lines connecting the data points are included to guide the eye.

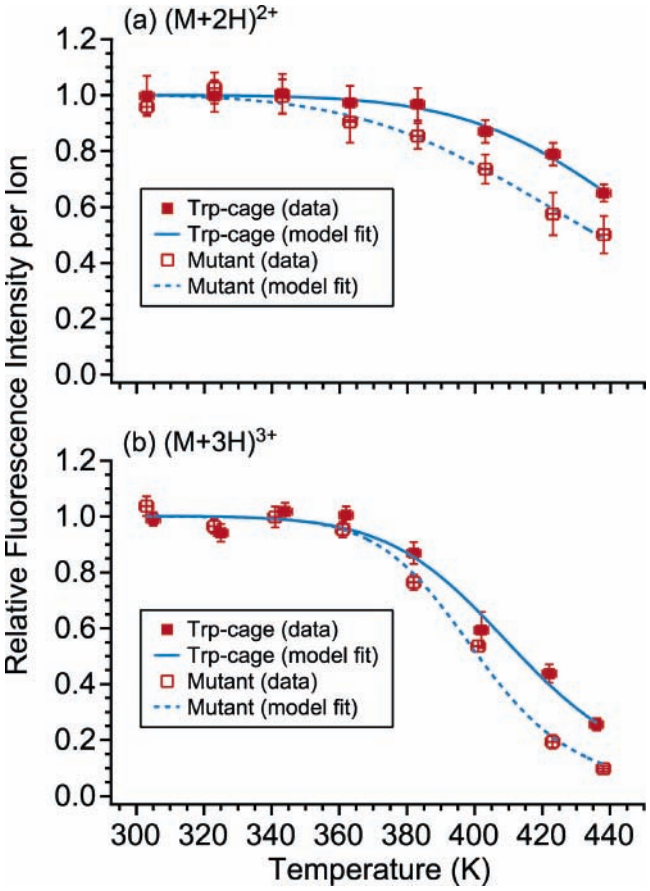

Figure 8. Normalized fluorescence intensity per ion vs temperature for the (a) $(M + 2H)^{2+}$ and (b) $(M + 3H)^{3+}$ ions of Trp-cage-BoTMR (closed squares) and the Trp-cage-BoTMR mutant in which Asp9 has been replaced by Asn (open squares). Model fits to the data are delineated by blue curves. Intensities are normalized to 303 K values.

TABLE 2: Differences between Thermochemical Parameters for Ions of BoTMR-derivatized Trp-cage and the Trp-cage Mutant in Which Asp9 Is Replaced with Asn

ion	$\Delta(\Delta H)$ (kJ/mol)	$\Delta(\Delta S)$ (J/mol·K)
$(M + 2H)^{2+}$	16 ± 12	29 ± 30
$(M + 3H)^{3+}$	17 ± 19	44 ± 48

The NMR structure[60] of Trp-cage suggests the existence of a (+ − +) salt bridge between Lys8, Asp9, and Arg16. Trp-cage variants in which Asp9 is replaced by Asn are poorly folded in solution, as demonstrated in our lab[71] and elsewhere,[60] indicating that the salt bridge is an important contributor to Trp-cage stability in solution. (The Asp side chain is a carboxylic acid which is negatively charged in solution but the Asn side chain is the analogous amide, which is not charged. The Asp9→Asn substitution breaks the + − + salt bridge by eliminating the negative charge.) In gas phase, however, the temperature-dependent fluorescence data of the $(M + 2H)^{2+}$ and $(M + 3H)^{3+}$ ions of the single-point Trp-cage mutant, Asp9→Asn, are similar to those of the unmutated ions (Figure 8) and the associated thermochemical parameters are the same within statistical uncertainty (Table 2). From this, we conclude that the salt bridge is *not* a significant contributor to the stability of these unsolvated ions with respect to the conformational change that occurs between 303 and 438 K. One possible explanation for this is that the salt bridge may cease to exist upon solvent removal (i.e., a proton may be transferred from the positively charged, protonated Lys8 to the negatively charged, deprotonated Asp9). Alternatively, it may be that the salt bridge exists in the unsolvated ions but is not broken during the conformational change that occurs over the temperature range investigated.

To definitively identify the occurrence of quenching in Trp-cage ions, *time-resolved* measurements of the fluorescence decays were performed as a function of temperature (the occurrence of quenching results in a shorter fluorescence decay time). As shown in Figure 9a, the measured decay time for the $(M + 3H)^{3+}$ ion is essentially unchanged between 303 and 363 K but then decreases from 10 to 7.7 ns upon further heating to 440 K. The change in decay time closely follows the change in fluorescence intensity for this ion (Figure 9b). Quenching also was observed in the $(M + 2H)^{2+}$ ions at higher temperatures (the measured decay time of the $(M + 2H)^{2+}$ ion at 440 K was 34% shorter than that measured at 303 K; data are not shown). The measured decay signals were fit with a stretched exponential and displayed multiexponential behavior that increased with temperature. This implies that the ensemble of fluorescing biomolecules was not homogeneous. In particular, the conformations for which the quenching rate, k_q, is comparable to the radiative rate (i.e., $k_q\tau_0 \approx 1$) may represent a minor fraction of the total fluorescence. In this case, the observed changes in intensity may be small even though quenching is present.

4.2. Polyproline Peptides: Quenching vs Dye−Charge Interactions. A more comprehensive understanding of the processes which can produce changes in the fluorescence intensity or decay time is necessary for the successful application of these measurements to arbitrary biomolecules and noncova-

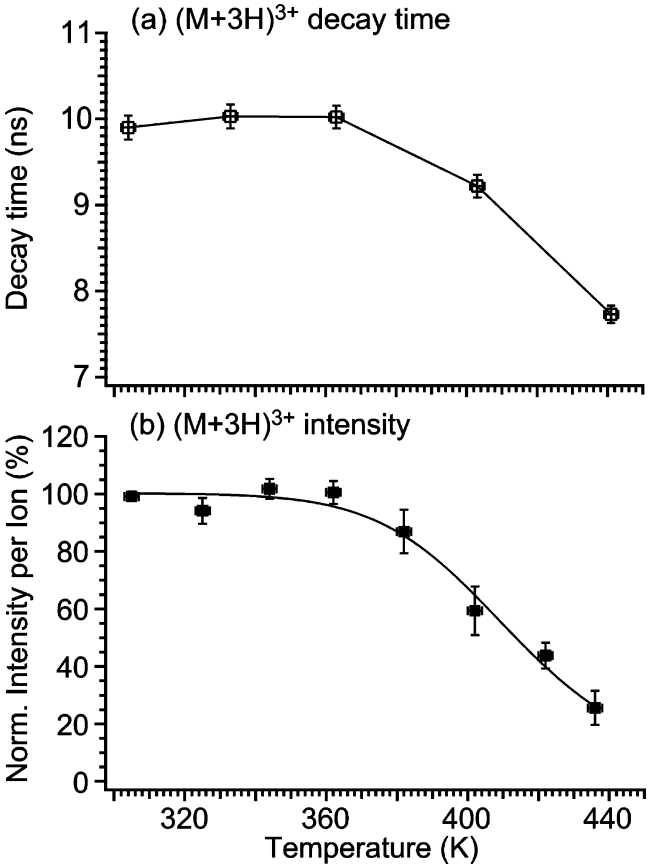

Figure 9. Comparison of (a) fluorescence decay time and (b) normalized fluorescence intensity per ion for the $(M + 3H)^{3+}$ ion of Trp-cage-BoTMR measured as a function of temperature. Lines between data points in (a) are included to guide the eye and the curve in (b) delineates the model fit to the data.

lent complexes. Measurements were performed on the derivatized peptides BoTMR−$(Pro)_n$-Arg-Trp ($n = 4$ or 10, "Pro_4" or "Pro_{10}", respectively) to study these processes independent of tertiary structure effects. The chemical structure is shown in Figure 10. Fluorescence intensities were measured at temperatures spanning the range of 303−438 K for each of the peptide ions of interest. At 303 K, the intensity of the $(M + H)^+$ ion of Pro_{10} is 18% lower than that of the corresponding ion of Pro_4, and the intensities of both ions decrease linearly with increasing temperature; however, the decrease is more rapid for Pro_4 than for Pro_{10} such that the intensities converge at the highest temperature investigated (Figure 11a). In contrast to the singly charged ions, for the $(M + 2H)^{2+}$ ions, the intensity of Pro_4 is 22% lower than that of Pro_{10} at 303 K, and the intensities of these ions decrease essentially in parallel upon heating to 438 K (Figure 11b). The rate of intensity decrease with increasing temperature is roughly 2 orders of magnitude higher in gas phase than in solution, consistent with the diffusion-limited kinetics of the dye−Trp interaction that exists in solution but not in gas phase.[39] To determine the extent to which the observed changes in fluorescence are caused by quenching by Trp, the experiments were repeated using the corresponding peptide ions which lack the C-terminal Trp residue. For the $(M + H)^+$ ions, the fluorescence intensities at a given temperature of Pro_4 and Pro_{10} without Trp are comparable with an intensity decrease of 55% between 303 and 438 K (Figure 12a). This result contrasts with the significantly different intensities observed for the $(M + H)^+$ ions of Pro_4 and Pro_{10}, with Trp at low temperatures (Figure 11a). For the $(M + 2H)^{2+}$ ions, the intensity order observed at all temperatures for the peptides with Trp, $Pro_{10} > Pro_4$, is also observed in the absence of Trp (Figure 12b). For all ions investigated, the rate of intensity decrease with increasing temperature is smaller for the peptide ions without Trp than for the corresponding ions with Trp (Table 3). Thus, the presence of Trp clearly affects the temperature-dependent fluorescence intensity of these peptide ions.

To definitively identify the occurrence of quenching by Trp, time-resolved measurements of the fluorescence decays were performed as a function of temperature. Example decays of Pro_4 $(M + H)^+$ ions at low and high temperatures and the instrument response function are shown in Figure 13. The instrument response function (Figure 13a; green curve) is generated from scattered excitation light and is measured to be ≤ 0.5 ns. The stretched exponential fits[80] shown in Figure 13 have beta values of ~1.0 at 303 K and 0.7 at 438 K indicating the multiexponential behavior characteristic of fluorescence from a heterogeneous ensemble.

The decay times of the $(M + H)^+$ ions of Pro_4 and Pro_{10} with Trp decrease 68 and 48%, respectively, over the temperature range 303−438 K (Figures 14a and 15a; red markers and lines), and the decay times of the respective $(M + 2H)^{2+}$ ions decrease 39 and 33% over this temperature range (Figures 14b and 15b). The shorter decay times observed at higher temperatures are consistent with increased conformational fluctuations that bring the dye and Trp into contact for quenching. The order of decay times, $Pro_{10} > Pro_4$, is maintained throughout the entire temperature range for the $(M + H)^+$ ion (Figures 14a and 15a); however, for the $(M + 2H)^{2+}$ ion, this is $Pro_{10} \approx Pro_4$ (Figures 14b and 15b). The apparent insensitivity of the decay time to chain length observed for the $(M + 2H)^{2+}$ ion may be because of the Coulombic repulsion between the two positive charges that restricts the dye−Trp interaction (the dye and Trp are located at opposite termini; Figure 10). The time-resolved measurements were repeated for identical polypeptides that do not have the Trp residue. In contrast to the large decreases in decay time observed upon heating the Trp-containing peptides, the decay times of the peptides without Trp decrease by less than 12% for both chain lengths, Pro_4 and Pro_{10} (Figures 14 and 15, respectively; blue markers and lines), and charge states, $(M + H)^+$ and $(M + 2H)^{2+}$.

For all of the work presented thus far, the BoTMR dye is attached to the peptide via a flexible aminohexanoate linker. Measurements were performed on peptides with Trp but without the linker to determine whether the measured decay time is sensitive to the decrease in accessible phase space that results from more closely coupling the dye to the polypeptide backbone. For the $(M + H)^+$ ions, the decay times of Pro_4 and Pro_{10} without the linker decrease by 37 and 31%, respectively, between 303 and 438 K (Figure 16a). These net decreases are smaller than those observed when the linker is present (68 and 48%, respectively; Figures 14a and 15a). For the $(M + 2H)^{2+}$ ions, the decay times of Pro_4 and Pro_{10} without the linker decrease by 29 and 19%, respectively, between 303 and 438 K (Figure 16b), again exhibiting smaller changes in decay time than when the linker is present (39 and 33%, respectively; Figure 14b and 15b). The smaller decreases in decay time observed in the absence of the linker are consistent with a decreased dye−Trp interaction because of an impaired ability of the dye to come into close contact with the Trp, which is located on the opposite terminus. Moreover, the increased rotational freedom provided by the flexible linker is expected to facilitate the formation of the optimum dye−Trp interaction geometry for quenching.[47] The decrease in decay time with increasing temperature appears to steepen at temperatures above 360 K (Figure 16a), possibly

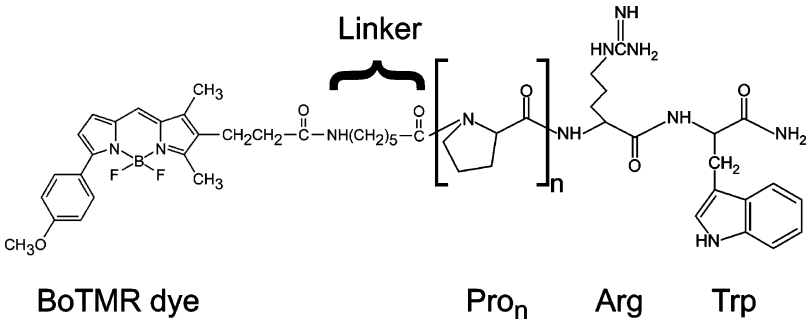

Figure 10. Chemical structure of the peptide Pro$_n$ (n = 4 or 10) derivatized with the dye BoTMR.

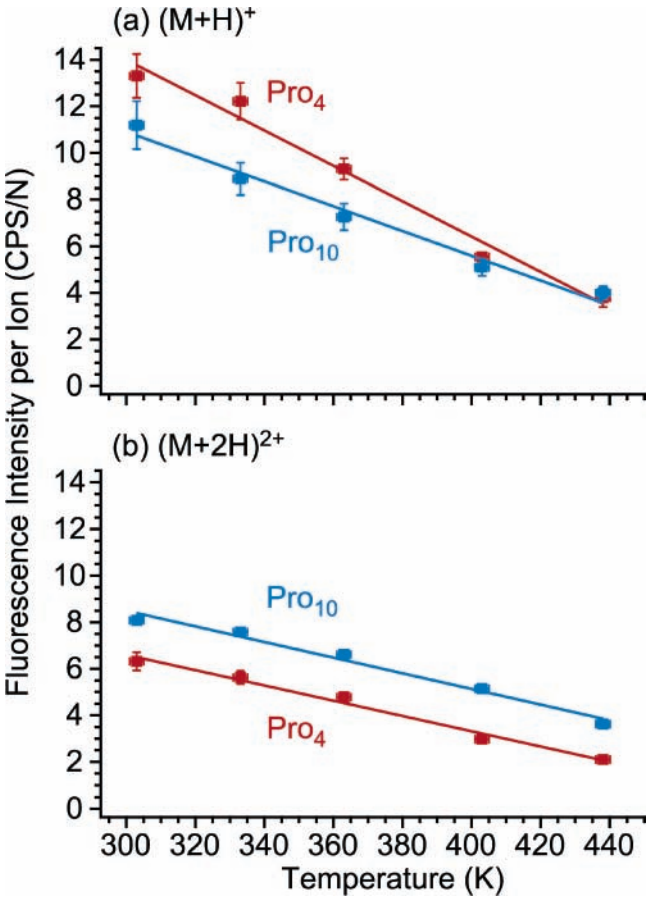

Figure 11. Fluorescence intensity per ion vs temperature for the (a) $(M + H)^+$ and (b) $(M + 2H)^{2+}$ ions of Pro$_4$ (red) and Pro$_{10}$ (blue) with best-fit lines to the data.

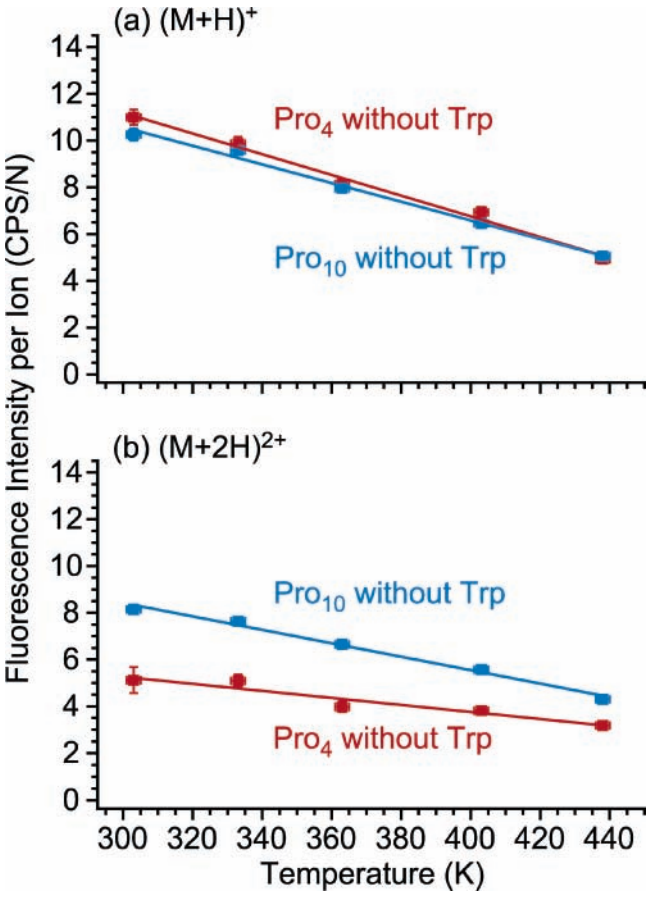

Figure 12. Fluorescence intensity per ion vs temperature for the (a) $(M + H)^+$ and (b) $(M + 2H)^{2+}$ ions of Pro$_4$ (red) and Pro$_{10}$ (blue) without Trp with best-fit lines to the data.

as a consequence of a conformational change that results in increased dye−Trp quenching interactions. In general, coupling the dye closely to the polypeptide backbone is expected to provide superior sensitivity to more subtle conformational changes, because the long, flexible linker has the effect of damping smaller polypeptide conformational fluctuations with respect to the fluorescent dye.

The time-resolved measurements presented here constitute the first definitive demonstration of fluorescence quenching by Trp in unsolvated peptides; however, another process besides quenching also is playing a role in the measured fluorescence as indicated by the significantly different *intensities* measured over a wide temperature range for different chain lengths of doubly charged ions that lack Trp (Figure 12b). This may be due to a dye−charge interaction. In the $(M + H)^+$ ions, the proton is most likely located on the Arg side chain near the C-terminus because of the high gas-phase basicity (GB) of Arg (1007 kJ/mol).[81] The exact location of the second proton in the $(M + 2H)^{2+}$ ion is not known; however, a reasonable location is near the N-terminus to minimize Coulombic repulsion. This would result in a closer dye−charge proximity in the $(M + 2H)^{2+}$ ions than in the $(M + H)^+$ ions, because the dye is located at the N-terminus.

TABLE 3: Slopes of Intensity vs Temperature for $(M + H)^+$ and $(M + 2H)^{2+}$ Ions of Poly(Pro) Peptides[a]

peptide	$(M + H)^+$ slope (CPS/N·K)[b]	$(M + 2H)^{2+}$ slope (CPS/N·K)[b]
Pro$_4$	−0.0758 ± 0.0059	−0.0328 ± 0.0022
Pro$_4$ without Trp	−0.0443 ± 0.0024	−0.0151 ± 0.0026
Pro$_{10}$	−0.0531 ± 0.0043	−0.0337 ± 0.0027
Pro$_{10}$ without Trp	−0.0398 ± 0.0021	−0.0288 ± 0.0017

[a] Stated errors are ± one standard deviation from the mean. [b] Slope of the best-fit line.

The results shown in Figures 14 and 15 not only identify Trp as the dominant quenching interaction but also suggest that

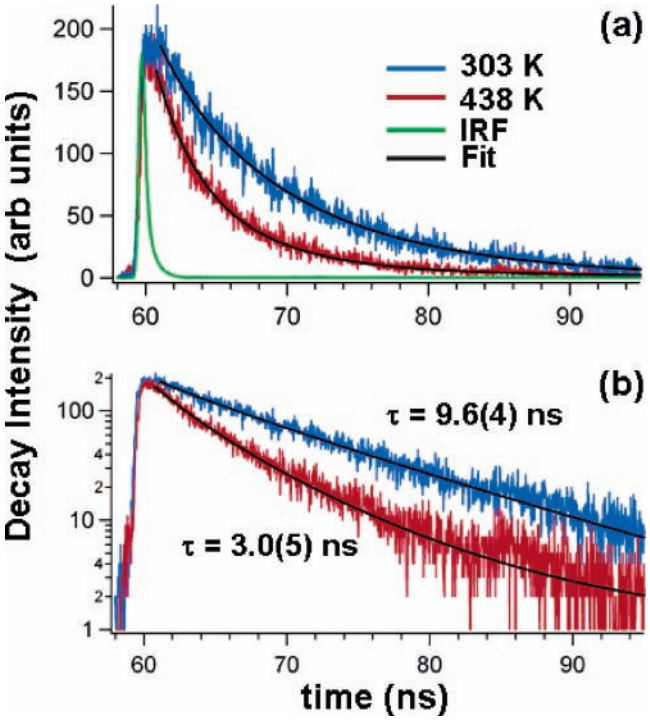

Figure 13. Example fluorescence decays of Pro_4 $(M + H)^+$ ions at 303 and 438 K (blue and red, respectively) and the instrument response function resulting from scattered excitation light (a; green). Fits to the measured decays by a stretched exponential model are delineated by black curves. Linear and logarithmic intensity scales are used in (a) and (b), respectively.

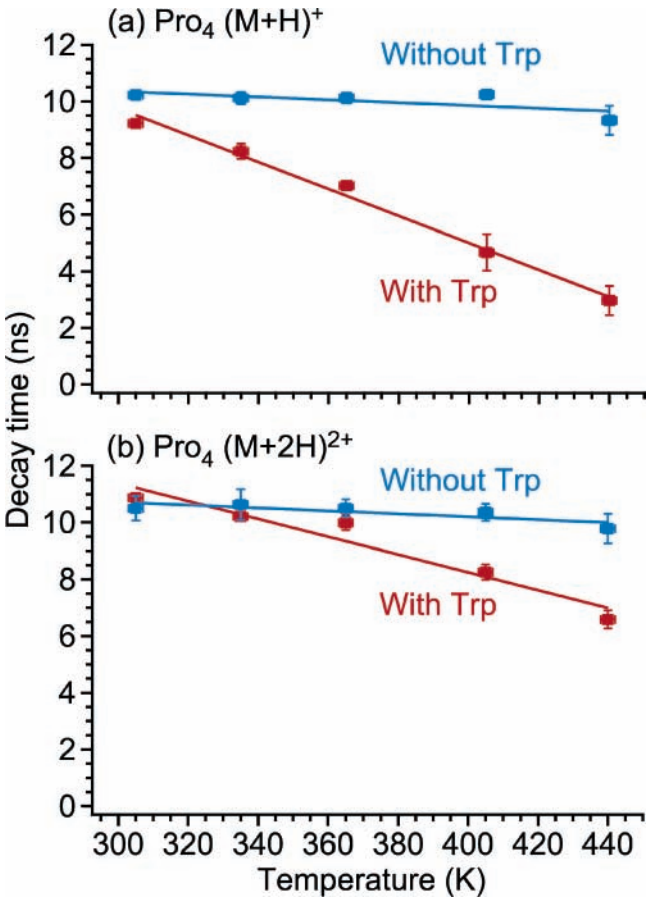

Figure 14. Fluorescence decay time vs temperature for the (a) $(M + H)^+$ and (b) $(M + 2H)^{2+}$ ions of Pro_4 with Trp (red) and without Trp (blue) with best-fit lines to the data.

the dye−charge interaction does not introduce significant quenching. However, the Coulomb fields of these charged residues can have a pronounced effect on the radiative absorption and emission[82,83] of the dye. Measurements of the Stark effect in solution[82,83] have been performed with external applied electric fields of $\sim 10^5-10^6$ V/cm.[84] However, in gas phase, the local Coulomb field strengths in biomolecular ions can be significantly higher, approaching $\sim 10^7-10^8$ V/cm, due to the lack of shielding by solvent. Stark effects can cause changes in absorption by inducing spectral shifts, level splitting, and changes in the transition-matrix element.

The shift of the absorption spectrum induced by the interaction of dyes with electrostatic fields can be estimated by considering the perturbation of the electronic ground and excited states, S_0 and S_1, respectively, through interactions of the field with the dipole moments associated with these states.[84−86] The energy separation, ΔE, introduced by the field, $\vec{E}$, is approximated as

$$\Delta E = E(S_0) - E(S_1) = -\Delta\vec{\mu}\cdot\vec{E} - \vec{E}\cdot\Delta\alpha\cdot\vec{E} \qquad (3)$$

where $\Delta\mu$ is the difference between the ground and excited-state dipole moments, and $\Delta\alpha$ is the difference in the polarizability tensor. Blue shifts of ~20 nm are estimated[39] for an average field of 2×10^7 V/cm based on parameters $\Delta\mu$ and $\Delta\alpha$ measured for the BODIPY core molecule.[87] A comparison between the measured emission spectrum of Pro_4 $(M + H)^+$ ions with that of BoTMR in hexane (Figure 17a) indicates a blue shift of the center wavelength of ~13 nm, which is comparable to the ~20 nm estimate. Emission spectra measured as a function of temperature (Figure 17b) indicate a shift to longer wavelengths and a slight increase of the bandwidth with increasing temperature. Conformational dynamics, which result in fluctuations of the Coulomb field strength at the dye position, produce a distribution of wavelength shifts about some mean determined by the average conformation. As a result, the temperature dependence of the emission spectrum will reflect these changes in conformational fluctuations through shifts of the emission peak wavelength and/or spectral broadening. Preliminary measurements of the dye-modified Trp-cage exhibit temperature-dependent spectral shifts and broadening, which are strongly dependent on charge state (data not shown). These spectral changes are related to increased fluctuations of the conformation with temperature that tend to reduce the effects of the Coulomb fields by averaging over angles implicit in Equation 3. The field-induced shifts of the dye absorption spectrum relative to the wavelength of the excitation laser (532 nm) would result in a decreased excitation rate and a consequent decrease in fluorescence intensity.

In addition to changing the absorption and emission spectra, there is a large body of evidence[88−93] that electric fields can strongly perturb the charge transfer process. In particular, the strong Coulomb fields arising from the relatively unshielded charges could significantly change the exothermicity of the charge-transfer reaction. In this case, there may be optimum separations that lead to efficient charge transfer and quenching of the dye fluorescence.

The underlying processes responsible for the variation in fluorescence intensity are highly dependent on the local fluctuations of the dye, Trp, and the charged residues. Consequently, these considerations reaffirm that these fluorescence measurements are related to the conformational fluctuations and not a static structure. Additional experiments and analysis are being pursued to help unravel these local interactions leading to the

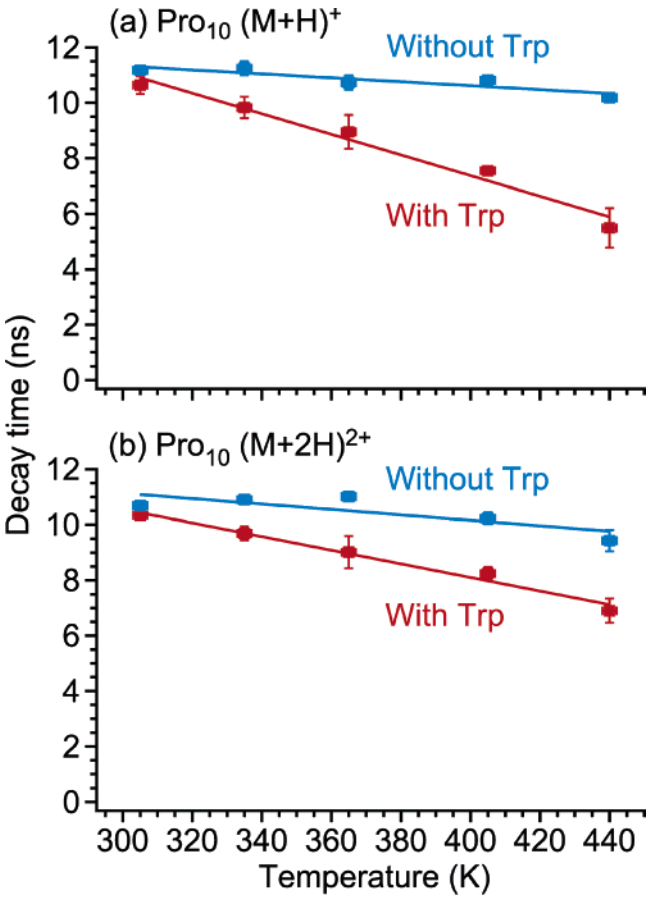

Figure 15. Fluorescence decay time vs temperature for the (a) $(M + H)^+$ and (b) $(M + 2H)^{2+}$ ions of Pro_{10} with Trp (red) and without Trp (blue) with best-fit lines to the data.

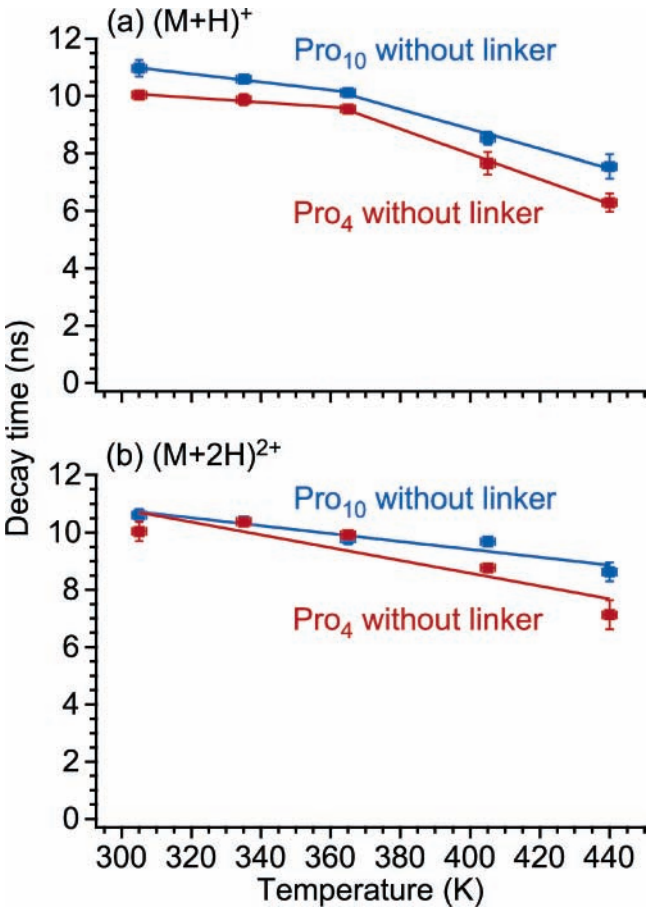

Figure 16. Fluorescence decay time vs temperature for the (a) $(M + H)^+$ and (b) $(M + 2H)^{2+}$ ions of Pro_4 (red) and Pro_{10} (blue) with Trp but without the flexible linker between the BoTMR dye and the peptide. In (a), best-fit lines to the first three and to the last three data points are shown for both Pro_4 and Pro_{10}, and in (b) lines have been fit to all data points for Pro_4 and Pro_{10}.

intensity variations, but the general conclusion remains clear that the fluorescence probe of conformational fluctuations can yield valuable information regarding biomolecule dynamics in gas phase.

4.3. β-Hairpin: Secondary Structure. The study of secondary structural elements such as α-helices and β-sheets has been expedited by the discovery of protein fragments and synthetic peptides, which assume such structures outside the environs of a larger protein.[94] We have investigated a synthetic peptide which assumes the minimal unit of an antiparallel β-sheet, a β-hairpin, in aqueous solution.[95] The conformation of this peptide is believed to be stabilized in part by hydrogen bonds formed between the two strands,[96] suggesting that the hairpin structure may be retained in gas phase in which hydrogen bonding is expected to be enhanced.[73,74] The sequence, H_2N-GEWTYDDATKTFTVTEK(BoTMR)-$CONH_2$, is the same as that used by Muñoz et al. for solution-phase laser temperature jump experiments,[96] except that the C-terminal lysine side chain is derivatized with BoTMR instead of dansyl. The quencher, Trp, and the BoTMR fluorophore are located near opposite termini, so the existence of the hairpin structure is expected to result in a certain amount of quenching because of the close dye-quencher proximity. Fraying or opening of the hairpin with increasing temperature should then result in an increase in fluorescence intensity and decay time because of the increase in dye−Trp separation and accompanying decrease in quenching. The fluorescence intensity per trapped $(M + 2H)^{2+}$ ion decreases by 10% as the temperature is increased from 303 to 363 K but then increases by 52% upon further heating to 438 K (Figure 18a). For the $(M + 3H)^{3+}$ ion, the intensity at 303 K is 83% higher than that of the $(M + 2H)^{2+}$ ion. The intensity of the $(M + 3H)^{3+}$ ion increases by 10% between 303 and 363 K but then *decreases* by 73% as the temperature is further increased to 438 K (Figure 18b). The intensity of the $(M + 4H)^{4+}$ ion at 303 K is a factor of 14 lower than that of the $(M + 3H)^{3+}$ ion. The intensity of this ion is essentially unchanged between 303 and 333 K but then decreases by 82% upon further heating to 438 K (Figure 18c). Thus, both the absolute intensities at 303 K and the changes in intensity with temperature differ dramatically for these three consecutive charge states of this peptide. The increase in intensity observed upon heating the $(M + 2H)^{2+}$ ion by itself is qualitatively consistent with some degree of retention of structure in gas phase that is opened up or frayed at higher temperatures (i.e., the measured ensembles may be mixtures of conformers of which some fraction exist with compact conformations). Whether this compact conformation retains a β-hairpin structure is uncertain.

To determine the extent to which the intensity changes of the $(M + 2H)^{2+}$ and $(M + 3H)^{3+}$ ions (Figure 18, panels a and b, respectively) are due to quenching, time-resolved fluorescence measurements were performed for these ions. For the $(M + 2H)^{2+}$ ion, the fluorescence decay times at 307 and 438 K are 10.8 (± 0.3) and 7.8 (± 0.2) ns, respectively (Figure 19). The long decay time measured at 307 K is comparable to that for peptides without Trp (Figures 14 and 15), suggesting the absence of significant quenching at this temperature, and the shorter decay time measured at 438 K indicates an increase in quenching

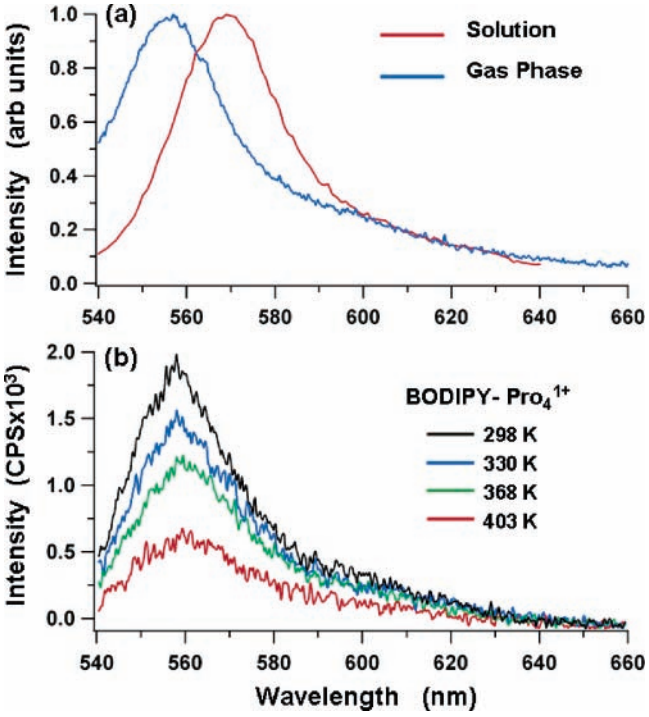

Figure 17. (a) Comparison of fluorescence emission spectra of BoTMR dye in hexane solution (red) with that of $(M + H)^+$ ions of Pro_4 (blue), both at ambient temperature. (b) Fluorescence emission spectra of $(M + H)^+$ ions of Pro_4 at 298, 330, 368, and 403 K (black, blue, green, and red, respectively).

with heating. Thus, the intensity increase observed upon heating the $(M + 2H)^{2+}$ ion (Figure 18a) is not due to a decrease in quenching of the dye by Trp. For the $(M + 3H)^{3+}$ ion, the fluorescence decay times at 307 and 438 K are 10.1 (± 0.2) and 9.1 (± 0.2) ns, respectively (Figure 19). Thus, the higher intensity observed at 303 K for the $(M + 3H)^{3+}$ ion (Figure 18b) than observed for the $(M + 2H)^{2+}$ ion (Figure 18a) does not appear to be because of a difference in quenching. Alternatively, the different intensities of these two charge states may be the result of dye−charge interactions. The β-hairpin is fragile (T_m = 297 K in aqueous solution)[96] and possibly may be altered by ionization and trapping.[97] In any case, our measurements indicate that the temperature-dependent conformational dynamics of this biomolecule depend profoundly on charge state. The locations of the ionizing protons are not known, although for the $(M + 2H)^{2+}$ ion, the N-terminus and the lysine at position 10 are reasonable guesses based on intrinsic basicity.[81] It is hoped that future measurements of the emission spectra as a function of temperature, to definitively identify charge-induced spectral shifts, combined with MD simulations of a variety of possible charge configurations, will provide further insight into the stability and dynamics of this basic element of secondary structure.

5. Summary and Conclusions

Fluorescence has been used for a long time to study protein conformational change in solution, but recently, we have applied this powerful, sensitive technique to monitoring structural changes or fluctuations in unsolvated protein and peptide ions confined to an RF ion trap. Unlike methods that characterize the overall molecular size, the fluorescence methodology detects conformational changes that result in alterations of the molecular environment surrounding a fluorescent dye that is attached to a specific site in the biomolecule under investigation. For unsolvated ions of the small protein, Trp-cage, the onset temperature for conformational change, as signaled by a decrease in fluorescence intensity, is lower for the $(M + 3H)^{3+}$ ion than for the $(M + 2H)^{2+}$ ion, consistent with an unfolding event that is promoted by greater Coulombic repulsion in the higher charge state. The energetics of the conformational change can be accounted for by a decrease in intramolecular hydrogen bonding as indicated by preliminary MD simulations. The data obtained for the Trp-cage mutant in which salt bridge formation is blocked (Asp9→Asn) differ only slightly from that of

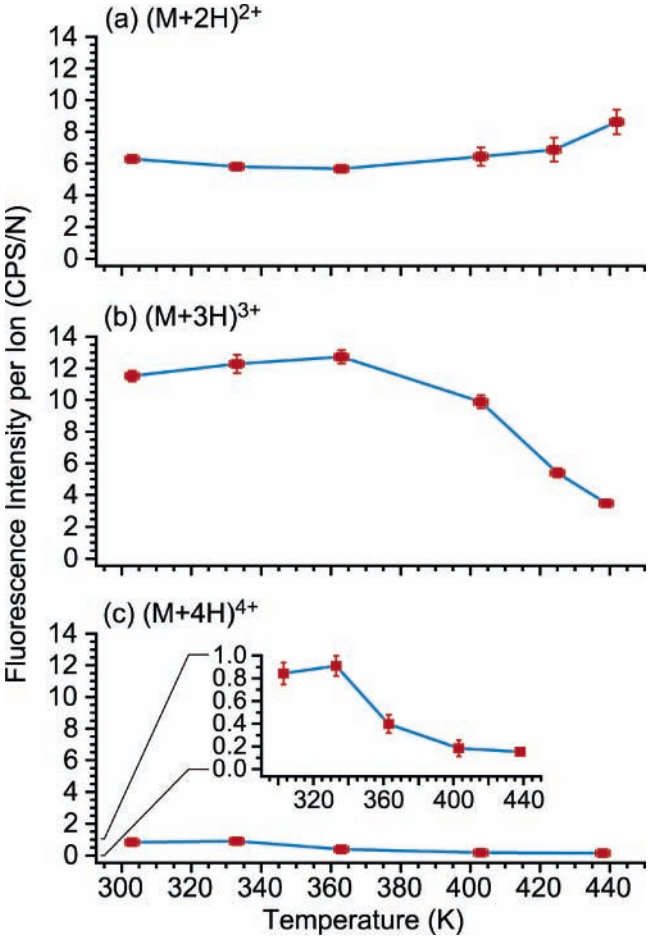

Figure 18. Fluorescence intensity per ion vs temperature for the (a) $(M + 2H)^{2+}$, (b) $(M + 3H)^{3+}$, and (c) $(M + 4H)^{4+}$ ions of the β-hairpin peptide. Measured data points are denoted by red markers and the blue lines connecting the data points are included to guide the eye. The inset in (c) shows the detail of the intensity change of the $(M + 4H)^{4+}$ ion.

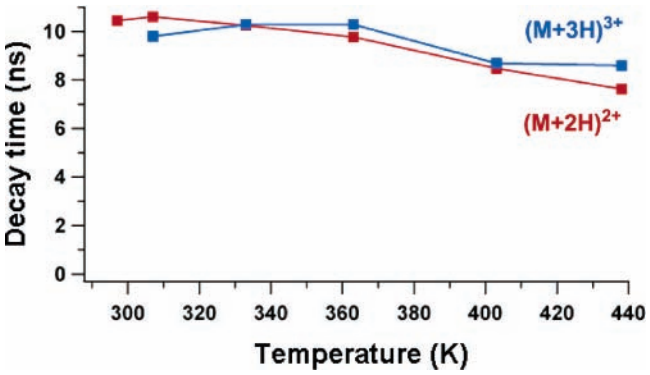

Figure 19. Fluorescence decay time vs temperature for the $(M + 2H)^{2+}$ (red) and (b) $(M + 3H)^{3+}$ (blue) ions of the β-hairpin peptide. The lines connecting the markers are included to guide the eye.

unmutated Trp-cage, indicating that the salt bridge (+ − +) which is critical for fold stability in solution does not provide a significant contribution to the stability in gas phase between 303 and 438 K.

Measurements of the fluorescence intensities, emission spectra, and decay times of small polyprolines unequivocally identify the occurrence of fluorescence quenching by tryptophan as well as the effects of a dye−charge interaction. The latter effect includes field-induced shifts in the excitation/emission spectra of the dye and alterations of the thermodynamic driving force for quenching. (The electrostatic fields in the unsolvated ions are estimated to be ∼1−2 orders of magnitude higher than those in solution because of the absence of shielding by solvent water.) Future experiments to distinguish between these two effects will use designed small peptides in which the separation between the charge and the dye is systematically varied.

The temperature-dependent fluorescence of a β-hairpin-forming peptide depends dramatically on charge state. The increase in fluorescence intensity with increasing temperature measured for the lowest charge state investigated, $(M + 2H)^{2+}$, is qualitatively consistent with some retention of a compact conformation in gas phase that is opened by heating. However, the measured decay times indicate that this phenomenon is not because of a decrease in quenching. MD simulations to provide insight into the conformational dynamics leading to the measured changes in fluorescence and the hairpin stability in gas phase are planned.

The experimental techniques described in this paper lay the foundation for using fluorescence measurements combined with theoretical calculations to probe the individual interactions that stabilize higher order structure of biomolecules and noncovalent complexes in the absence of the complicating effects of a solvent. All of our work thus far has focused on small sequences (<22 residues) to ensure that the experiments can be complemented by reliable and reasonably fast MD simulations; however, the methods outlined here can in principle be extended to larger species and noncovalent complexes.

Acknowledgment. The successful development of these fluorescence methods relied on the accomplishments of former postdoctoral fellows Professor Allison Danell (East Carolina University), Dr. Ryan Danell, Dr. Joseph Khoury, and Dr. Sandra Rodriguez-Cruz. The authors gratefully acknowledge Professor Rebecca Jockusch (University of Toronto) for assistance with measurements of the β-hairpin peptide, Ms. Alexandra Patriksson and Professor David van der Spoel (Uppsala University) for MD simulations, Dr. Joshua Edel and Professor Amit Meller (Boston University) for their advice on time-resolved fluorescence, Professors David Clemmer and Martin Jarrold (Indiana University) for useful discussions, Mr. Chris Stokes (Rowland) for assistance with setting up the time-resolved fluorescence apparatus, and the Rowland Institute at Harvard for generous funding.

References and Notes

(1) Creighton, T. E. *Proteins: Structures and Molecular Properties*, 2nd Ed.; W. H. Freeman: New York, 1993.

(2) Fersht, A. *Structure and Mechanism in Protein Science.: A Guide to Enzyme Catalysis and Protein Folding*; W. H. Freeman: New York, 1999.

(3) Szymkowski, D. *Curr. Opin. Drug Discovery Dev.* **2005**, *8*, 590−600.

(4) Cohen, F. E. *J. Mol. Biol.* **1999**, *293*, 313−320.

(5) Soto, C. *Nat. Rev. Neurosci.* **2003**, *4*, 49−60.

(6) Stefani, M. *Biochim. Biophys. Acta* **2004**, *1739*, 5−25.

(7) Jahn, T. R.; Radford, S. E. *FEBS J.* **2005**, *272*, 5962−5970.

(8) Karplus, M.; McCammon, J. A. *Nat. Struct. Biol.* **2002**, *9*, 646−652.

(9) Moraitakis, G.; Purkiss, A. G.; Goodfellow, J. M. *Rep. Prog. Phys.* **2003**, *66*, 383−406.

(10) Wysocki, V. H.; Resing, K. A.; Zhang, Q.; Cheng, G. *Methods (Orlando, Florida)* **2005**, *35*, 211−222.

(11) Bogdanov, B.; Smith, R. D. *Mass Spectrom. Rev.* **2005**, *24*, 168−200.

(12) Kelleher, N. L.; Zubarev, R. A.; Bush, K.; Furie, B.; Furie, B. C.; McLafferty, F. W.; Walsh, C. T. *Anal. Chem.* **1999**, *71*, 4250−4253.

(13) Shi, S. D.-H.; Hemling, M. E.; Carr, S. A. *Anal. Chem.* **2001**, *73*, 19−22.

(14) Tsaprailis, G.; Nair, H.; Somogyi, A.; Wysocki, V. H.; Zhong, W.; Futrell, J. H.; Summerfield, S. G.; Gaskell, S. J. *J. Am. Chem. Soc.* **1999**, *121*, 5142−5154.

(15) Horn, D. M.; Breuker, K.; Frank, A. J.; McLafferty, F. W. *J. Am. Chem. Soc.* **2001**, *123*, 9792−9799.

(16) Iavarone, A. T.; Williams, E. R. *Anal. Chem.* **2003**, *75*, 4525−4533.

(17) Adams, C. M.; Kjeldsen, F.; Zubarev, R. A.; Budnik, B. A.; Haselmann, K. F. *J. Am. Soc. Mass Spectrom.* **2004**, *15*, 1087−1098.

(18) Fenn, J. B.; Mann, M.; Meng, C. K.; Wong, S. F.; Whitehouse, C. M. *Science* **1989**, *246*, 64−71.

(19) Karas, M.; Bachmann, D.; Bahr, U.; Hillenkamp, F. *Int. J. Mass Spectrom. Ion Processes* **1987**, *78*, 53−68.

(20) Tanaka, K.; Waki, H.; Ido, Y.; Akita, S. *Rapid Commun. Mass Spectrom.* **1989**, *3*, 436−439.

(21) Kinnear, B. S.; Hartings, M. R.; Jarrold, M. F. *J. Am. Chem. Soc.* **2001**, *123*, 5660−5667.

(22) Badman, E. R.; Hoaglund-Hyzer, C. S.; Clemmer, D. E. *Anal. Chem.* **2001**, *73*, 6000−6007.

(23) Myung, S.; Badman, E. R.; Lee, Y. J.; Clemmer, D. E. *J. Phys. Chem. A* **2002**, *106*, 9976−9982.

(24) Kaleta, D. T.; Jarrold, M. F. *J. Am. Chem. Soc.* **2003**, *125*, 7186−7187.

(25) Bernstein, S. L.; Wyttenbach, T.; Baumketner, A.; Shea, J.-E.; Bitan, G.; Teplow, D. B.; Bowers, M. T. *J. Am. Chem. Soc.* **2005**, *127*, 2075−2084.

(26) Robinson, E. W.; Williams, E. R. *J. Am. Soc. Mass Spectrom.* **2005**, *16*, 1427−1437.

(27) Gross, D. S.; Schnier, P. D.; Rodriguez-Cruz, S. E.; Fagerquist, C. K.; Williams, E. R. *Proc. Natl. Acad. Sci. U.S.A.* **1996**, *93*, 3143−3148.

(28) McLafferty, F. W.; Guan, Z.; Haupts, U.; Wood, T. D.; Kelleher, N. L. *J. Am. Chem. Soc.* **1998**, *120*, 4732−4740.

(29) (a) Dunbar, R. C. *Mass Spectrom. Rev.* **2004**, *23*, 127−158. (b) Price, W. D.; Schnier, P. D.; Williams, E. R. *Anal. Chem.* **1996**, *68*, 859−866.

(30) Zubarev, R. A.; Kelleher, N. L.; McLafferty, F. W. *J. Am. Chem. Soc.* **1998**, *120*, 3265−3266.

(31) Syka, J. E. P.; Coon, J. J.; Schroeder, M. J.; Shabanowitz, J.; Hunt, D. F. *Proc. Natl. Acad. Sci. U.S.A.* **2004**, *101*, 9528−9533.

(32) Oh, H.; Breuker, K.; Sze, S. K.; Ge, Y.; Carpenter, B. K.; McLafferty, F. W. *Proc. Natl. Acad. Sci. U.S.A.* **2002**, *99*, 15863−15868.

(33) Oomens, J.; Polfer, N.; Moore, D. T.; van der Meer, L.; Marshall, A. G.; Eyler, J. R.; Meijer, G.; von Helden, G. *Phys. Chem. Chem. Phys.* **2005**, *7*, 1345−1348.

(34) Khoury, J. T.; Rodriguez-Cruz, S. E.; Parks, J. H. *J. Am. Soc. Mass Spectrom.* **2002**, *13*, 696−708.

(35) Danell, A. S.; Parks, J. H. *Int. J. Mass Spectrom.* **2003**, *229*, 35−45.

(36) Danell, A. S.; Parks, J. H. *J. Am. Soc. Mass Spectrom.* **2003**, *14*, 1330−1339.

(37) Danell, A. S.; Danell, R. M.; Parks, J. H. In *Clusters and Nano-Assemblies Physical and Biological Systems*, Jena, P.; Khanna, S. N.; Rao, B. K., Eds.; World Scientific Publishing Co.: Singapore, 2005.

(38) Iavarone, A. T.; Parks, J. H. *J. Am. Chem. Soc.* **2005**, *127*, 8606−8607.

(39) Iavarone, A. T.; Meinen, J.; Schulze, S.; Parks, J. H. *Int. J. Mass Spectrom.* **2006**, 253, 172−180.

(40) Lapidus, L. J.; Eaton, W. A.; Hofrichter, J. *Proc. Natl Acad. Sci. U.S.A.* **2000**, *97*, 7220−7225.

(41) Thompson, P. A.; Muñoz, V.; Jas, G. S.; Henry, E. R.; Eaton, W. A.; Hofrichter, J. *J. Phys. Chem. B* **2000**, *104*, 378−389.

(42) Jas, G. S.; Eaton, W. A.; Hofrichter, J. *J. Phys. Chem. B* **2001**, *105*, 261−272.

(43) Hagen, S. J.; Carswell, C. W.; Sjolander, E. M. *J. Mol. Biol.* **2001**, *305*, 1161−1171.

(44) Hudgins, R. R.; Huang, F.; Gramlich, G.; Nau, W. M. *J. Am. Chem. Soc.* **2002**, *124*, 556−564.

(45) Marmé, N.; Knemeyer, J.-P.; Sauer, M.; Wolfrum, J. *Bioconjugate Chem.* **2003**, *14*, 1133−1139.

(46) Neuweiler, H.; Schulz, A.; Böhmer, M.; Enderlein, J.; Sauer, M. *J. Am. Chem. Soc.* **2003**, *125*, 5324−5330.

(47) Vaiana, A. C.; Neuweiler, H.; Schulz, A.; Wolfrum, J.; Sauer, M.; Smith, J. C. *J. Am. Chem. Soc.* **2003**, *125*, 14564−14572.
(48) Yang, H.; Luo, G.; Karnchanaphanurach, P.; Louie, T.-M.; Rech, I.; Cova, S.; Xun, L.; Xie, X. S. *Science* **2003**, *302*, 262−266.
(49) Jones, G., II.; Zhou, X.; Vullev, V. I. *Photochem. Photobiol. Sci.* **2003**, *2*, 1080−1087.
(50) Huang, F.; Hudgins, R. R.; Nau, W. M. *J. Am. Chem. Soc.* **2004**, *126*, 16665−16675.
(51) Royer, C. A. *Chem. Rev.* **2006**, *106*, 1769−1784.
(52) (a) Doose, S.; Neuweiler, H.; Sauer, M. *ChemPhysChem.* **2005**, *6*, 2277−2285. (b) Neuweiler, H.; Doose, S.; Sauer, M. *Proc. Natl. Acad. Sci. U.S.A.* **2005**, *102*, 16650−16655.
(53) Hopfield, J. J. *Proc. Natl. Acad. Sci. U.S.A.* **1974**, *71*, 3640−3644.
(54) Moser, C. C.; Keske, J. M.; Warncke, K.; Farid, R. S.; Dutton, P. L. *Nature (London)* **1992**, *355*, 796−802.
(55) Guan, S.; Marshall, A. G. *Int. J. Mass Spectrom. Ion Processes* **1996**, *157/158*, 5−37; Marshall, A. G.; Wang, T.-C. L.; Ricca, T. L. *J. Am. Chem. Soc.* **1985**, *107*, 7893−7897.
(56) (a) Julian, R. K., Jr.; Cooks, R. G. *Anal. Chem.* **1993**, *65*, 1827−1833. (b) Soni, M. H.; Cooks, R. G. *Anal. Chem.* **1994**, *66*, 2488−2496.
(57) Website: Invitrogen-Molecular Probes, URL: http://probes.invitrogen.com, accessed 8/1/06.
(58) Patriksson, A.; Adams, C.; Kjeldsen, F.; Raber, J.; van der Spoel, D.; Zubarev, R. A. *Int. J. Mass Spectrom.* **2006**, *248*, 124−135.
(59) Lindahl, E.; Hess, B. A.; van der Spoel, D. *J. Mol. Model.* **2001**, *7*, 306−317.
(60) Neidigh, J. W.; Fesinmeyer, R. M.; Andersen, N. H. *Nat. Struct. Biol.* **2002**, *9*, 425−430.
(61) Hukushima, K.; Nemoto, K. *J. Phys. Soc. Jpn.* **1996**, *65*, 1604−1608.
(62) Simmerling, C.; Strockbine, B.; Roitberg, A. E. *J. Am. Chem. Soc.* **2002**, *124*, 11258−11259.
(63) Snow, C. D.; Zagrovic, B.; Pande, V. S. *J. Am. Chem. Soc.* **2002**, *124*, 14548−14549.
(64) Pitera, J. W.; Swope, W. *Proc. Natl. Acad. Sci. U.S.A.* **2003**, *100*, 7587−7592.
(65) Chowdhury, S.; Lee, M. C.; Xiong, G. M.; Duan, Y. *J. Mol. Biol.* **2003**, *327*, 711−717.
(66) Zhou, R. *Proc. Natl. Acad. Sci. U.S.A.* **2003**, *100*, 13280−13285.
(67) Seshasayee, A. S. N. *Theor. Biol. Med. Modell.* **2005**, *2*, 7.
(68) Ding, F.; Buldyrev, S. V.; Dokholyan, N. V. *Biophys. J.* **2005**, *88*, 147−155.
(69) Using intrinsic Trp fluorescence (268 nm excitation).
(70) Qiu, L.; Pabit, S. A.; Roitberg, A. E.; Hagen, S. J. *J. Am. Chem. Soc.* **2002**, *124*, 12952−12953.
(71) Iavarone, A. T.; Patriksson, A.; van der Spoel, D.; Parks, J. H. *J. Am. Chem. Soc.*, submitted for publication 2006.
(72) Schnier, P. D.; Gross, D. S.; Williams, E. R. *J. Am. Chem. Soc.* **1995**, *117*, 6747−6757.
(73) Wolynes, P. G. *Proc. Natl. Acad. Sci. U.S.A.* **1995**, *92*, 2426−2427.
(74) Kitova, E. N.; Bundle, D. R.; Klassen, J. S. *J. Am. Chem. Soc.* **2002**, *124*, 5902−5913.
(75) Grabowski, S. J. *J. Phys. Org. Chem.* **2004**, *17*, 18−31.
(76) Meot-Ner, M. *Chem. Rev.* **2005**, *105*, 213−284.
(77) Strittmatter, E. F.; Williams, E. R. *J. Phys. Chem. A* **2000**, *104*, 6069−6076.
(78) Strittmatter, E. F.; Wong, R. L.; Williams, E. R. *J. Phys. Chem. A* **2000**, *104*, 10271−10279.
(79) Strittmatter, E. F.; Williams, E. R. *Int. J. Mass Spectrom.* **2001**, *212*, 287−300.
(80) Klafter, J.; Shlesinger, M. F. *Proc. Natl. Acad. Sci. U.S.A.* **1986**, *83*, 848−851.
(81) Hunter, E. P.; Lias, S. G. In *NIST Chemistry WebBook, NIST Standard Reference Database*, Number 69; Linstrom, P. J.; Mallard, W. G., Eds., National Institute of Standards and Technology: Gaithersburg, MD, 2005.
(82) Liptay, W. In *Electronic States*; Lim, E. C., ed.; Academic Press: New York, 1974; Vol. 1, 129.
(83) Bublitz, G. U.; Boxer, S. G. *Annu. Rev. Phys. Chem.* **1997**, *48*, 213−242.
(84) Asamoah, O. K.; Wuskell, J. P.; Loew, L. M.; Bezanilla, F. *Neuron* **2003**, *37*, 85−98.
(85) Kuhn, B.; Fromherz, P.; Denk, W. *Biophys. J.* **2004**, *87*, 631−639.
(86) Sczepan, M.; Rettig, W.; Tolmachev, A. I. *Photochem. Photobiol. Sci.* **2003**, *2*, 1264−1271.
(87) Bergström, F.; Mikhalyov, I.; Hägglöf, P.; Wortmann, R.; Ny, T.; Johansson, L. B.-A. *J. Am. Chem. Soc.* **2002**, *124*, 196−204.
(88) (a) Hilczer, M.; Traytak, S.; Tachiya, M. *J. Chem. Phys.* **2001**, *115*, 11249−11253. (b) Hilczer, M.; Tachiya, M. *J. Chem. Phys.* **2002**, *117*, 1759−1767.
(89) Boxer, S. G.; Goldstein, R. A.; Lockhart, D. J.; Middendorf, T. R.; Takiff, L. *J. Phys. Chem.* **1989**, *93*, 8280−8294.
(90) Lockhart, D. J.; Kirmaier, C.; Holten, D.; Boxer, S. G. *J. Phys. Chem.* **1990**, *94*, 6987−6995.
(91) Lao, K. Q.; Franzen, S.; Steffen, M.; Lambright, D.; Stanley, R.; Boxer, S. G. *Chem. Phys.* **1995**, *197*, 259−275.
(92) Tsushima, M.; Ohta, N. *J. Chem. Phys.* **2004**, *120*, 6238−6245.
(93) (a) Callis, P. R.; Liu, T. *Chem. Phys.* **2006**, *326*, 230−239. (b) Callis, P. R.; Vivian, J. T. *Chem. Phys. Lett.* **2003**, *369*, 409−414.
(94) Galzitskaya, O. V.; Higo, J.; Finkelstein, A. V. *Curr. Protein Pept. Sci.* **2002**, *3*, 191−200.
(95) Blanco, F. J.; Rivas, G.; Serrano, L. *Nat. Struct. Biol.* **1994**, *1*, 584−590.
(96) Muñoz, V.; Thompson, P. A.; Hofrichter, J.; Eaton, W. A. *Nature (London)* **1997**, *390*, 196−199.
(97) Clemmer, D. E.; Jarrold, M. F., private communication.